Archive of SID.ir

Investigation of TiO_2 Concentration and Calcination Temperature Effects on Hybrid Membrane Properties for Wastewater Treatment

Abed, Yakine; Zrelli, Adel*+; Chaouachi, Bechir

Laboratory of Energy, Water, Environment, and Process, LR18ES35,
National Engineering School of Gabes, University of Gabes, Gabes, TUNISIA

ABSTRACT: *In recent years, hybrid membranes have been developed to address the need for membranes with excellent chemical and thermal resistance. In this study, we present the preparation of a hybrid flat membrane using a dip-coating process with clay and titanium dioxide (TiO_2). We investigated two parameters: TiO_2 concentration and calcination temperature. We also evaluated the performance of the resulting membranes in treating colored wastewater. Our results show that increasing TiO_2 concentration from 1 to 21 g/L enhances the hydrophilicity of the membrane, as evidenced by a decrease in contact angle. The mass of TiO_2 fixed on the membrane surface also increases, leading to a similar contact angle for 11 and 21 g/L. Notably, TiO_2 nanoparticles were adsorbed onto the membrane pores resulting in reduced membrane porosity. The average permeate fluxes decreased with increasing TiO_2 concentration. We also observed a decline in methylene blue degradation rate with the increase of TiO_2 concentration from 11 to 21 g/L. The maximum methylene blue degradation rate was achieved with a membrane coated with 11 g/L of TiO_2. Moreover, we studied the effect of calcination temperature on membrane properties. Interestingly, increasing the calcination temperature from 300°C to 600°C did not significantly alter the contact angle. The highest methylene blue degradation rate (86.04%) was achieved with 11 g/L TiO_2 at a calcination temperature of 300 °C. The prepared flat membranes demonstrated promising performance in treating colored wastewater, highlighting their potential for efficient wastewater treatment applications.*

KEYWORDS: *Ceramic membrane; Characterization; TiO_2; Wastewater; Treatment.*

INTRODUCTION

Water pollution caused by wastewater containing various contaminants, such as toxic species, organic and inorganic chemicals, minerals, sediments and dyes, is a major environmental concern. Dyes like methyl orange and methylene blue, commonly used in the textile, printing, pharmaceuticals and research industries, generate large volumes of wastewater [1,2], which are non-biodegradable and not effectively treated using traditional methods such as adsorption on activated carbon, coagulation, sedimentation, chemical oxidation and

* *To whom correspondence should be addressed.*
+ *E-mail: adel.zrelli@yahoo.fr*
1021-9986/2024/3/1183-1193 11/$/6.01

Archive of SID.ir

Archive of SID.ir

biological digestion [3,4]. In the studies conducted by *Zhang et al*. [5] and *Lin et al*. [6], it has been observed that the adsorption capacity of TiO_2 is limited due to its small specific surface area. Moreover, the separation of TiO_2 particles from water after the adsorption process poses significant challenges. To overcome these limitations, photocatalyse-utilizing TiO_2 has emerged as a promising technique, benefiting from its high stability, amphoteric character, and large band gap energy [7]. However, a major obstacle for the widespread application of the photocatalytic process arises when TiO_2 is immersed in wastewater for treatment: the efficient removal of the photocatalyse (TiO_2) from the treated water [8,9]. Hence, it is imperative to pursue the creation of an intelligent system capable of efficiently removing low concentration contaminants from wastewater. The preference lies in membranes that exhibit superior selectivity and permeability when separating solvent mixtures. Considering the industrial perspective, the presence of high solvent flux membranes holds great significance. Such membranes can play a pivotal role in the design of new processes by substantially diminishing capital expenditure requirements [10]. The combination of membrane technology and photocatalysis has emerged as a promising approach for efficient and sustainable water treatment. In one study, a polysulfone membrane was incorporated with TiO_2 to investigate the degradation of eosin yellow dye under the visible light irradiation [11]. In another study, TiO_2 was immobilized on laccase, a plant material, to evaluate its ability to break down reactive dyes in textiles [12]. Polymeric membranes lack the thermal and chemical stability exhibited by inorganic membranes. Consequently, inorganic membranes are more widely used due to their long lifetime. Porous ceramic membranes, which offer benefits such as thermal, chemical and mechanical resistance, and controllable microstructure, have been of interest to the scientific community. However, their use in wastewater treatment is limited by their high cost. Thus, current research on the development of low-cost membranes that combine adsorption and photocatalysis, providing a novel and sustainable approach to water treatment technology [13]. Clays have been widely used as support materials due to their low cost, abundant availability, high cation exchange capacity, porosity, high surface area, swelling, and good binding properties [14]. Titanium dioxide has been immobilized on these ceramic substrates through various methods, such as in situ hydrothermal processes [15], electrospinning [16] , sol-gel process [17], self-assembly [18], photoassisted deposition, solvent casting and grafting [19]. TiO_2-coated ceramic membranes have been shown to be effective in the degradation of dyes. This is due to the photocatalytic properties of --TiO_2, which is a well-known semiconductor material. When exposed to ultraviolet (UV) light, TiO_2 can generate electron-hole pairs. These electron-hole pairs can then react with dyes to form reactive oxygen species (ROS), such as hydroxyl radicals. ROS are highly reactive and can oxidize dyes, breaking them down into smaller, less harmful compounds. The degradation process continues until the dyes are completely degraded [20].

The objective of this study was to investigate the potential impact of calcination temperature and TiO_2 concentration on membrane characteristics, permeate flux, and methylene blue degradation. To the best of our knowledge, no prior research has examined the influence of these two parameters, namely calcination temperature and TiO_2 concentration, on both membrane characteristics and the efficiency of methylene blue degradation.

EXPERIMENTAL SECTION

Material

Clay was obtained from the southern Tunisian region of Matmata-Gabes-Tunisia. Palm stone, an organic waste product derived from date palm trees, was used as pore-forming. Distilled water was employed as a solvent for the ceramic paste preparation. Furthermore, TiO_2 was purchased from LoBA Chemie.

Clay characterization

Particle Size Analysis

The particle size distribution of clay was determined by a laser diffraction apparatus (Malvern Panalytical, Mastersizer 3000, UK) equipped with a dry powder disperser (Aero S). Measurements were performed in triplicate, at 25 °C.

Fourier Transform Infrared spectroscopy analysis of clay powder and sintered clay

Fourier transform infrared (FT-IR) analysis of clay powder and sintered clay was performed using a Spectrum Two (PerkinElmer, USA) FT-IR spectrometer. The spectrometer was mounted with a diamond Attenuated Total

Archive of SID.ir

Archive of SID.ir

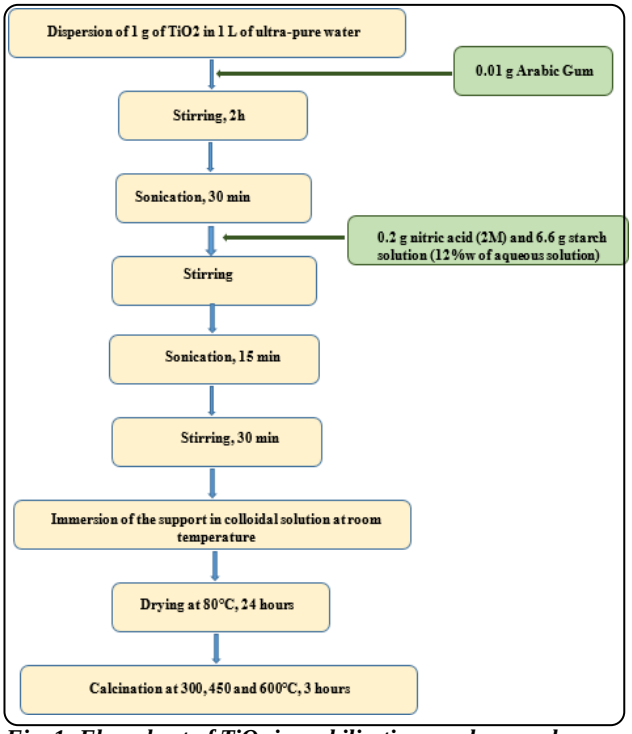

Fig. 1: Flow chart of TiO_2 immobilization on clay membranes.

Reflectance (ATR) accessory. Spectra were recorded in the wave numbers range of 450-4000 cm^{-1} by an average of 4 scans at a spectral resolution of 2 cm^{-1}.

Ceramic membrane preparation

The clay was grinded using a grinder to achieve a high degree of fineness in the resulting powder. The sieving process was then carried out, and the particles obtained had diameters ranging from 63 to 80 µm [21,22]. A plastic paste was synthesized using ceramic powder, organic additions, and water. The paste was composed of 67 wt% mineral powder, 4 wt% starch, 4 wt% palm stone powder, and 25 wt% water. A flat configuration membrane with a porous structure was fabricated using the compression method. Sintering experiments were conducted in a muffle furnace using a two-step process, with the first step at 250°C, followed by the second step at 1000°C. The temperature-time profile played a crucial role in determining the porous volume, pore diameters, morphology, and mechanical strength of the membrane.

TiO_2/clay ceramic membrane preparation

A dip-coating process was employed to coat clay membranes with TiO_2 solution at different concentrations (1, 11, and 21 g/L). The coated membranes were dried

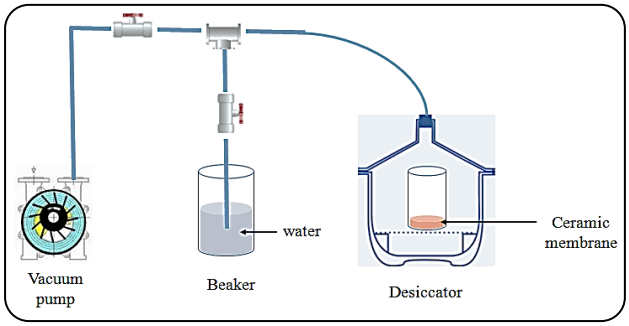

Fig. 2: Porosity measuring set-up.

in an oven at 80°C for 24 hours to remove residual moisture. Subsequently, the membranes were calcinated in a muffle furnace for three hours at various temperatures (300, 450, and 600°C). Fig. 1 illustrates the process of TiO_2/clay membrane preparation.

Ceramic membrane characterization

Porosity and pore size

The membrane's porosity was evaluated using the Archimedes method [23,24] with water as the wetting liquid, as illustrated in Fig. 2. To account for variations in membrane dimensions, we measured different masses and used these values to calculate the membrane porosity. The porosity ε was determined using the following Eq. (1):

$$\varepsilon(\%) = \frac{V_{PO}}{V_S} x100 \qquad (1)$$

Where, V_{PO} is the open pores volume of the ceramic membrane; and V_S is the real volume of the ceramic membrane.

The Mean pore radius r_{mean} was determined by the filtration velocity method. According to Guerout–Elford Ferry equation, r_{mean} could be determinate by the Eq. (2) [25,26]:

$$r_{mean} = \sqrt{\frac{(2{,}9 - 1{,}75\,\varepsilon) x\, 8\,\eta\, l\, Q}{\varepsilon.\, A.\, \Delta P}} \qquad (2)$$

Where η is water viscosity (8,9 x 10^{-4} Pa s); l is the membrane thickness (m); ΔP is the operation pressure, ε is the porosity, and Q is the permeate flow (m^3/s).

Contact angle

To assess the wettability of the ceramic membrane, contact angle tests were performed using a KRÜSS Drop Shape Analyzer – DSA25 as a measuring device. The sessile drop method was used to determine the wettability of the membrane by dropping model liquid, such as water,

Archive of SID.ir

Archive of SID.ir

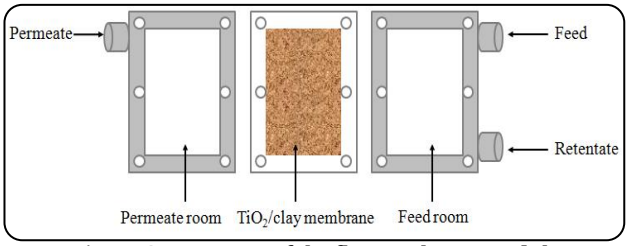

Fig. 3: Components of the flat membrane module.

onto the surface. Contact angles were measured using water, which allowed us to deduce the hydrophobic character (angle higher than 90°, low surface energy) or hydrophilic character (angle lower than 90°, high surface energy) of the surface [27].

Conception of pilot unit of membrane photocatalysis and experimental protocol of methylene blue degradation

The surface area of the photocatalytic ceramic membrane measures 102 cm^2. To assess the membrane's performance, it was incorporated into a flat membrane module, as depicted in Fig. 3. The solution was exposed to irradiation using a SYLVANIA UV lamp. In order to prevent the entry of visible light into the reactor and the escape of ultraviolet light, the reactor was fully covered with cardboard. To initiate the photocatalytic reaction, a solution of methylene blue, with a pH of 5.7 and a concentration of $2x10^{-5}$ mol/L, was prepared and then poured into the feed tank of the installation. The pump operated in a closed circuit, circulating the solution between the reactor and the tank, as illustrated in Fig. 4. The solution samples are collected at 30-minute intervals throughout a three-hour treatment period. Subsequently, the samples are stored in a lightless environment and analyzed using UV-vis spectrophotometry at a wavelength of λmax = 660 nm. The spectrophotometer used for this purpose is a Perkin Elmer brand. All experiments were done at a constant room temperature of 25°C. The permeation flux (J, $m^3/m^2 \cdot h$) was calculated by Eq. (3):

$$J = \frac{V}{At} \qquad (3)$$

Where *V*, *A* and *t* represent the permeate volume, the membrane surface and the time respectively. The efficiency of the photodegradation treatment of methylene blue can be calculated by Eq. (4):

$$R\,(\%) = \frac{C_0 - C_t}{C_0} \times 100 \qquad (4)$$

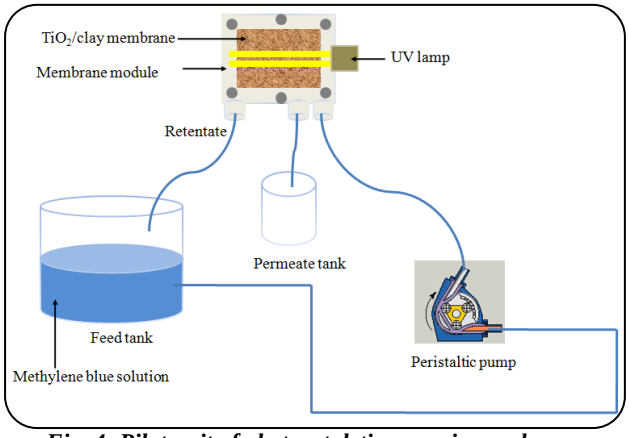

Fig. 4: Pilot unit of photocatalytic ceramic membrane.

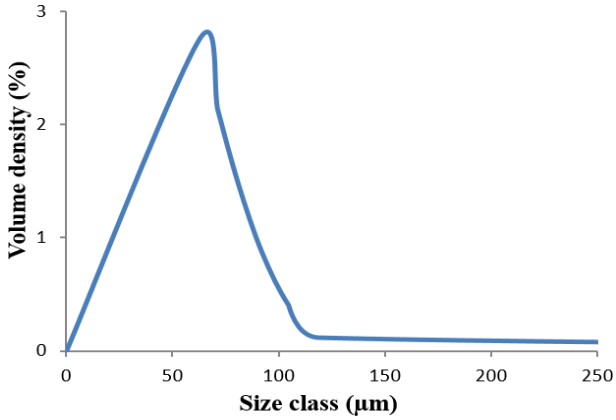

Fig. 5: Particle size distribution of clay particles.

Where, C_t is the concentration of methylene blue at the selected time and C_0 is the initial concentration of methylene blue of feed.

RESULTS AND DISCUSSION

Particle size analysis

After the clay grinding process, a sieving procedure was carried out, and a granulometric analysis was conducted on the resulting fraction. The particle size distribution of the clay is presented in Fig. 5, revealing a pronounced peak around 64 µm. This peak confirms the successful sieving process and indicates that the majority of particles fall within the desired size range (63 µm < particle diameter < 80 µm).

Fourier Transform Infrared spectroscopy analysis of clay powder

To determine the composition of the functional groups present in the raw materials, Fourier Transform InfraRed

Archive of SID.ir

Archive of SID.ir

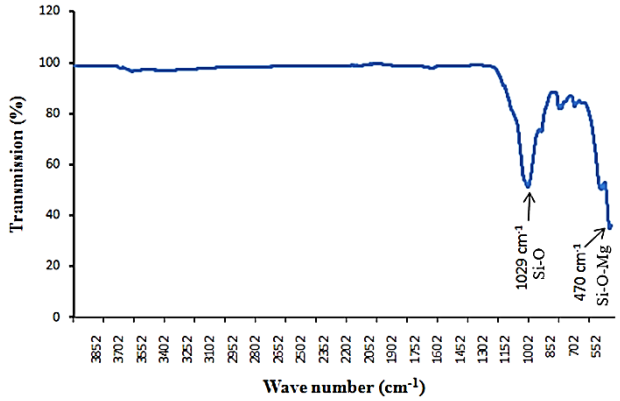

Fig. 6: FT-IR spectrum of the clay powder.

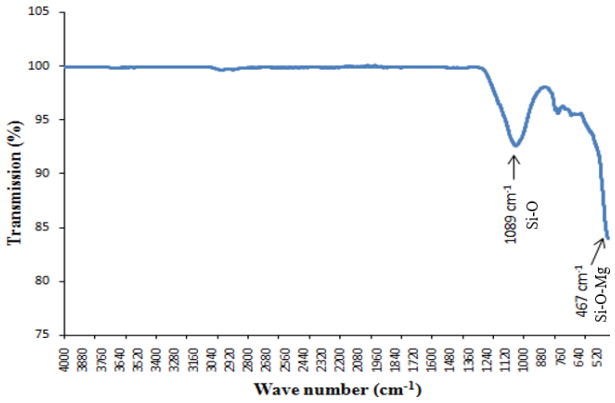

Fig. 7: FT-IR spectrum of sintered clay.

(FT-IR) spectroscopy analysis was conducted. The resulting spectrum of the clay powder is displayed in Fig. 6, exhibiting two prominent characteristic bands. The band at 1029 cm^{-1} is assigned as the valence band associated with Si-O vibration. Additionally, the vibrational band observed at 914 cm^{-1} is attributed to the deformation of the Al-OH bond, while the band at 695 cm^{-1} corresponds to different modes of the Si-O-Al bond. Furthermore, the peak at 497 cm^{-1} is identified as Si-O-Al bending vibrations. Lastly, the band located at 470 cm^{-1} represents the deformation vibration of the Si-O-Mg bond [27,28].

Factors affecting methylene blue photodegradation

Inspired by various studies on the photodegradation of organic pollutants in water [29,30], this experimental study explores the impact of two operating parameters, namely the TiO_2 concentration and the calcination temperature on TiO_2 fixed mass, contact angle, porosity, average permeate flux, and methylene blue degradation. The obtained results are reported in the following sections.

Effect of calcination temperature and TiO_2 concentration on TiO_2 fixed mass

Fig. 8 depicts the influence of calcination temperature and TiO_2 concentration on TiO_2 fixed mass. The synthesis parameters were set to 300-600°C and 1-21 g/L, respectively. As the calcination temperature increases, the TiO_2 fixed mass initially rises and then falls. Specifically, for 1 g/L of TiO_2, the fixed mass increases by 77.46% as the temperature ascends from 300 to 600°C before dropping by 58.22%. For 11 g/L, the TiO_2 fixed mass rises by 85.60% and declines by 58.22%. In the case of the highest concentration of 21 g/L, the fixed mass of TiO_2

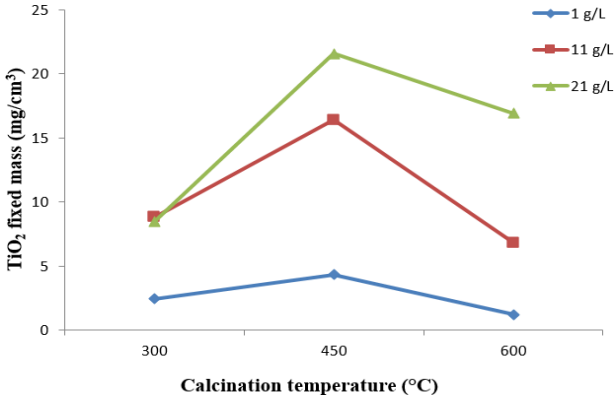

Fig. 8: Effect of calcination on the mass of fixed TiO_2.

exhibits an increase from 8.41 mg/cm^3 to 21.55 mg/cm^3 as the calcination temperature rises from 300 to 450°C. However, at a temperature of 600°C, the fixed mass decreases to 16.09 mg/cm^3. This is due to the increased firmness of the TiO_2 nanoparticles caused by changes in the surface fabric property of clay and growth in the TiO_2 crystal structure, which raises the TiO_2 content. However, excessively high calcination temperatures lead to the sintering of the TiO_2 particles, causing the film to shrink, crack, or debond from the substrate, resulting in a decrease in TiO_2 fixed mass. These findings align with those reported in [31]. Fig. 8 demonstrates that increasing the TiO_2 concentration increased the fixed mass of TiO_2. This observation is consistent with photos of clay membranes coated with varying concentrations of TiO_2 as shown in Fig. 9. When TiO_2 nanoparticles were immobilized onto the clay membrane, a chemical interaction between the TiO_2 nanoparticles and SiO_2 in the clay membrane occurred through Si-O-Ti bonding. This interaction facilitated a uniform distribution of TiO_2 nanoparticles

Archive of SID.ir

Archive of SID.ir

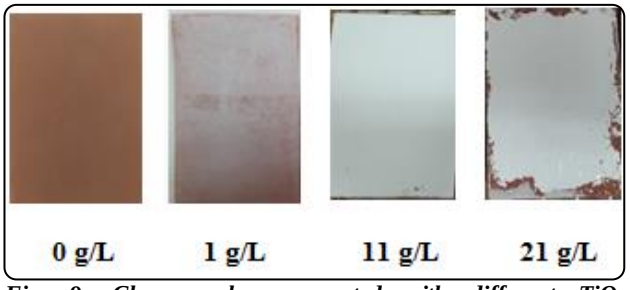

Fig. 9: Clay membranes coated with different TiO_2 concentration at 300 °C.

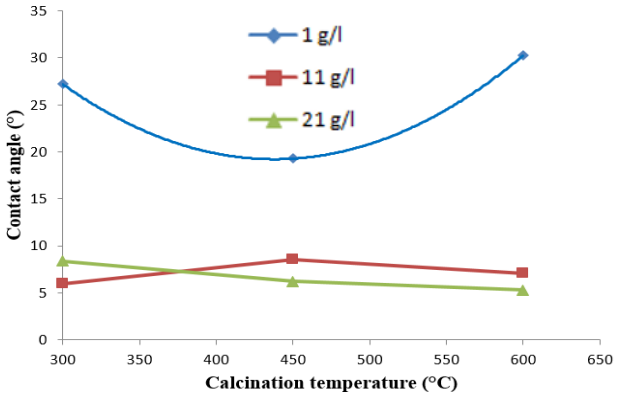

Fig. 10: Effect of calcination temperature on membrane contact angle.

in the clay membrane, as was the case for the membrane coated with 11 g/L of TiO_2 [32]. However, as shown in Fig. 9, the membrane coated with 21 g/L of TiO_2 was not covered with TiO_2 nanoparticles. This phenomenon can be attributed to the occurrence of debonding or crack formation, which becomes more prominent with increasing TiO_2 concentration [33,34].

Effect of calcination temperature and TiO_2 concentration on membrane contact angle

The calcination temperature was varied from 300 to 600°C while the TiO_2 concentrations were varied from 1 to 21 g/L. The results indicate that an increase in TiO_2 concentration led to a decrease in contact angle, indicating improved hydrophilicity of the membrane. As seen in Fig. 10, a higher TiO_2 concentration of 21 g/L resulted in the lowest contact angle. Additionally, an increase in calcination temperature from 300 to 600 °C led to an increase in TiO_2 fixed mass, resulting in similar contact angle values for 11 and 21 g/L concentrations. The presence of TiO_2 nanoparticles on the membrane surface, as confirmed by Fig. 9, significantly reduced the contact angle

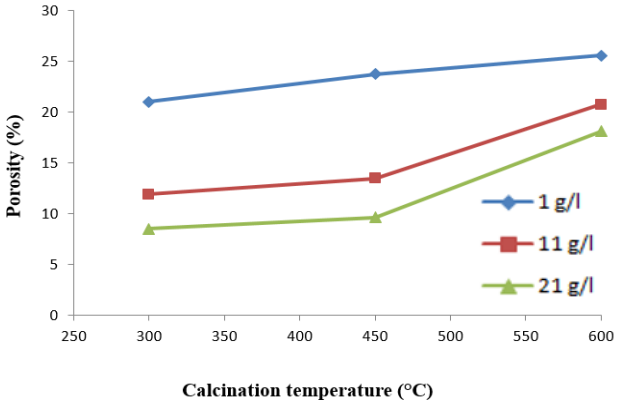

Fig. 11: Effect of calcination on the porosity.

to approximately 7° [35] indicating high hydrophilicity. However, at a TiO_2 concentration of 1 g/L, the contact angle increased, indicating a lower hydrophilic behavior of the membrane. Furthermore, the hydrophilic nature of the membrane surface enhances its affinity for contaminants, such as methylene blue, leading to improved adsorption and facilitating better contact with the photocatalytic material. As a result, this promotes the adsorption of organic pollutants onto the membrane surface, thereby facilitating subsequent photocatalytic degradation.

Effect of calcination temperature and TiO_2 concentration on membrane porosity

Fig. 11 shows the impact of calcination temperature and TiO_2 concentration on the membrane porosity. It can be observed that the porosity of the membrane varies with the increasing TiO_2 content. The findings suggest that an increase in TiO_2 concentration results in a gradual decrease in the open porosity of the membrane due to the adsorption of TiO_2 nanoparticles on the surface of the membrane pores. This, in turn, reduces the surface area of the pores and leads to a decline in membrane porosity. The results are consistent with those presented in Fig. 8, where an increase in TiO_2 concentration leads to an increase in TiO_2 fixed mass at all calcination temperatures. As shown in Fig. 9, the TiO_2 nanoparticles cover almost every part of the membrane surface, leading to a decrease in porosity. Similarly, as the calcination temperature increases from 300 to 600°C, the porosity of the membranes declines significantly for all calcination temperatures due to the entry of TiO_2 nanoparticles into the membrane pores, partially blocking some of them. The high concentration of TiO_2 (Fig. 11) causes a decline in porosity due to the agglomeration of

Archive of SID.ir

Archive of SID.ir

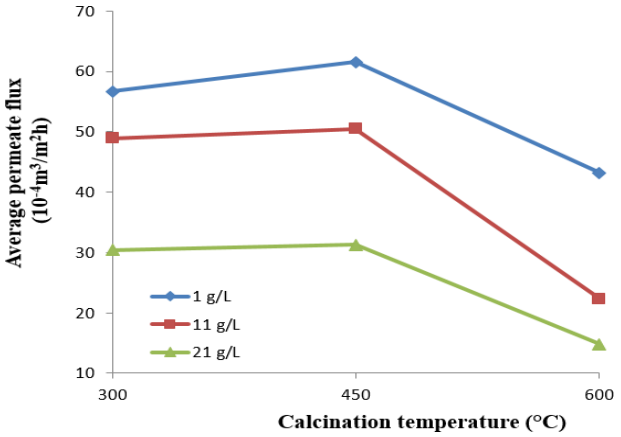

Fig. 12: Effect of calcination temperature on the permeate flux.

TiO_2 nanoparticles on the membrane surface, which can be detached from the membrane during calcination, resulting in a higher porosity and poor compactness.

Effect of calcination temperature and TiO_2 concentration on average permeate flux:

This study aimed to evaluate the performance of flat ceramic membranes for the filtration process. Specifically, the average permeate flux and TiO_2 concentration were examined as a function of calcination temperatures, and the results are presented in Fig. 12. The findings showed that the permeation flux of all prepared membranes decreased as the TiO_2 concentration increased from 1 g/L to 21 g/L. This decrease suggested that the permeation flux tended to become restricted with increasing TiO_2 concentration, consistent with previous research [36]. The cake layer formed on the membrane surface initially caused low resistance to permeation. However, as the layer cake thickened, it behaved with high resistance to permeation, resulting in a reduction in the permeation flux. This phenomenon may be partly attributed to the interactions between the membranes and the methylene blue solution, particularly with the decrease of the cross-section during the cross-flow filtration [37]. In addition, we found that increase in the calcination temperature led to a decrease in the permeation fluxes. This reduction may be attributed to the increase in TiO_2 crystallite size, resulting in densification and phase transformation from anatase to rutile. Notably, the maximum permeation fluxes were observed at 450 °C, and some researchers suggested that at this temperature, there is a maximum percentage of anatase titania present, which generates minimum densification in the membrane [38]. An alternative explanation can be derived from Fig. 13, which depicts the progression of average permeate flux as a function of $\frac{r_{mean}\ X\ Porosity}{Thickness}$ at various calcination temperatures. This graph exhibits a similar trend as shown in Fig. 12. So, the maximum ratio of $\frac{r_{mean}\ X\ Porosity}{Thickness}$ is proved at 450°C.

Effect of calcination temperature on degradation of methylene blue in retentate:

This part investigates the photoactivity of methylene blue on TiO_2 by examining the photocatalytic activity of samples calcined at 300-600°C under UV irradiation. The results are displayed in Fig. 14. Based on Fig. 8, we found that as the calcination temperature increased from 300°C to 450°C, the TiO_2 fixed mass was improved, especially for membranes coated with 21 g/L of TiO_2, which showed the highest evolution of TiO_2 fixed mass. Consequently, the removal efficiency of methylene blue corresponding to the membrane coated with 21 g/L was the lowest when the calcination temperature increased from 300 to 600°C. In addition, the removal efficiency of methylene blue increased as the calcination temperature increased from 450°C to 600°C. This increase was attributed to the energy band gap variation, which decreased as the calcination temperature increased from 450°C to 600°C. This finding was consistent with previous research [39]. As seen, operating at 300°C led to higher degradation of methylene blue, which is 77.12, 86.04 and 70.15% for TiO_2 concentrations of 1, 11 and 21 g/L, respectively. The impact of calcination temperature on the degradation of methylene blue can be attributed to the influence of temperature on catalyst particle size, as reported by *Potti et al*. [40] and *Li et al*. [41]. These studies indicate that lower calcination temperatures result in the formation of catalysts with smaller particle sizes. Typically, smaller particle sizes of TiO_2 demonstrate higher activity compared to larger particles [42–44]. This enhancement in activity can be attributed to several factors. Firstly, smaller particles offer a larger surface area per unit mass, facilitating improved interaction between TiO_2 and the reactants. Consequently, this increased surface area provides a greater number of active sites for reactions, thereby enhancing activity. Moreover, smaller particles possess a higher proportion of surface atoms, resulting in an increased availability of reactive sites for chemical

Archive of SID.ir

Archive of SID.ir

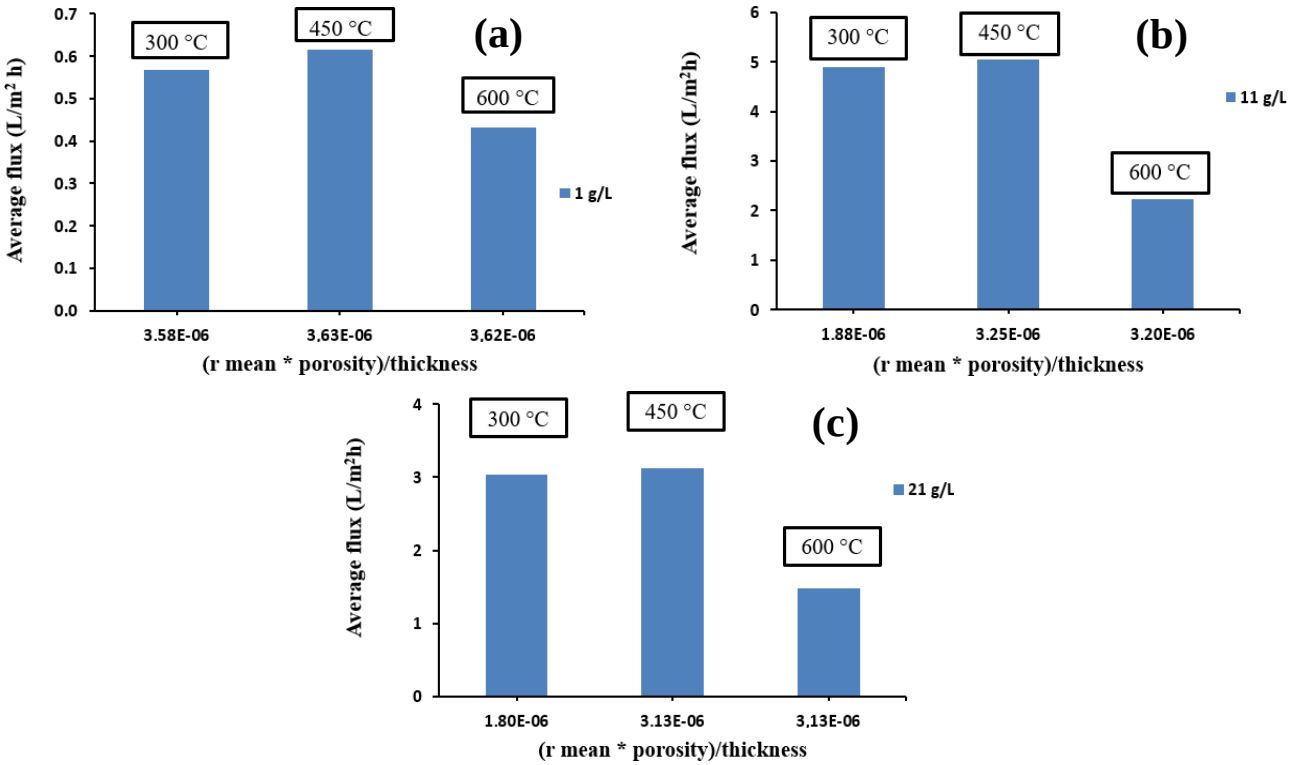

Fig. 13: Effect of (r mean*porosity)/thickness on calcination temperature and average permeate flux for a TiO_2 concentration of (a) 1 g/L, (b) 11 g/L and (c) 21 g/L.

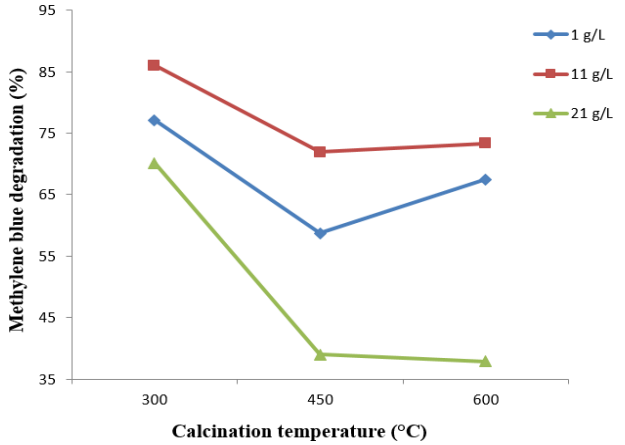

Fig. 14: Methylene blue degradation VS calcination temperature.

reactions, ultimately contributing to enhanced dye removal [45]. Additionally, smaller particle sizes reduce the diffusion path length for both reactants and products, leading to accelerated mass transfer and promoting more efficient reaction kinetics [46]. Based on these observations, an increase in calcination temperature is associated with an increase in TiO_2 particle sizes and a decrease in methylene blue degradation.

A comparative analysis was performed, comparing our findings with previous studies, as outlined in the below table. The comparison reveals a strong agreement between our results and the findings reported in existing literature.

CONCLUSIONS

In this study, we employed the dip-coating technique was employed to modify the clay membranes with titanium dioxide. This investigation examined the impact of TiO_2 concentration and calcination temperature on various parameters, including TiO_2 fixed mass, membrane contact angle, porosity, average permeate flux, and methylene blue degradation. As calcination temperature increased from 300°C to 600°C, we observed changes in TiO_2 fixed mass due to sintering, affecting membrane integrity. The addition of titanium dioxide enhanced membrane hydrophilicity, as evidenced by a significantly reduced contact angle of 7°. However, increasing TiO_2 concentration led to reduced membrane porosity due to TiO_2 nanoparticles adsorption on the surface of the membrane pores. Permeate flux exhibited variations with changing TiO_2 concentration, with maximum fluxes observed at 450°C. The most efficient methylene blue

Archive of SID.ir

Archive of SID.ir

Table 1: A Comparative Analysis of Our Results with Literature Data

Membrane Material	Calcination Temperature (°C)	Type of light	Dye	Degradation (%)	References
Polyacrylonitrile Polyamide 6	-	Without light	Methylene blue	73	[47]
aluminum nitrate nonahydrate calcium nitrate tetrahydrate cerium(III) nitrate hexahydrate zirconyl chloride octahydrate	650	UV	Methylene blue	90.7	[48]
	750	Sunlight	Methylene blue	88.5	
α–Alumina supports γ–alumina	500	UV	Methylene blue	72	[49]
				82	
Metakaolin	500	UV	Methylene blue	93	[50]
TiO_2	300	UV	Methylene blue	80	[51]
Clay	300	UV	Methylene blue	86	This study

degradation, at rate of 86.04%, was achieved with TiO_2 concentrations of 11 g/L at 300℃.

In light of our findings, it is essential to acknowledge the limitations of our study, including the specific conditions and materials used. Future research directions may explore the practical application of this technique in water treatment, particularly in the context of treating water contaminated with antibiotics. Additionally, considering the potential cost-effectiveness of utilizing solar radiation instead of UV lamps for abatement is a promising avenue for further investigation.

Received : May 23, 2023 ; Accepted : Sep. 25, 2023

REFERENCES

[1] Bennabi S., Mahammed N., Kinetic and Thermodynamic Study of Methyl Orange Dye Adsorption on Zinc Carbonyldiphthalate, an Organometallic-Based Material Prepared with a Montmorillonite Clay, *Iran. J. Chem. Chem. Eng. (IJCCE)*, **42(1):** 123–138 (2022).

[2] Nath A., Mishra A., Pande P.P., Shankar R., Synthesis of Disaccharide-Based Xanthates for the Removal of Some Heavy Metals from Aqueous Solution, *Iran. J. Chem. Chem. Eng. (IJCCE)*, **41(4):** 1137–1150 (2022).

[3] Zhang G.K., Ding X.M., He F.S., Yu X.Y., Zhou J., Hu Y.J., Xie J.W., Low-Temperature Synthesis and Photocatalytic Activity of TiO_2 Pillared Montmorillonite, *Langmuir*, **24(3):** 1026-1030 (2008).

[4] Zhang Y., Wang D., Zhang G., Photocatalytic Degradation of Organic Contaminants by TiO_2/Sepiolite Composites Prepared at Low Temperature, *Chem. Eng. J.*, **173(1):** 1–10 (2011).

[5] Zhang Y., Gan H., Zhang, G., A novel Mixed-Phase TiO_2/Kaolinite Composites and their Photocatalytic Activity for Degradation of Organic Contaminants, *Chem. Eng. J.*, **172(2):** 936–943 (2011).

[6] Lin X.-Z., Ma T.-Y., Yuan Z.-Y., Titania–Silica–Phosphonate Triconstituent Hybrid Mesoporous Materials as Adsorbents in Gas and Liquid Phases, *Chem. Eng. J.*, **166(3):** 1144–1151 (2011).

[7] Fatimah I., Wang S., Narsito., Wijaya K., Composites of TiO_2-Aluminum Pillared Montmorillonite: Synthesis, Characterization and Photocatalytic Degradation of Methylene Blue, *Appl. Clay Sci.*, **50(4):** 588–593 (2010).

[8] Zhang H., Quan X., Chen S., Zhao H., Zhao Y., Fabrication of Photocatalytic Membrane and Evaluation its Efficiency in Removal of Organic Pollutants from Water, *Sep. Purif. Technol.*, **50(2):** 147–155 (2006).

[9] Choi H., Stathatos E., Dionysiou D.D., Photocatalytic TiO_2 Films and Membranes for the Development of Efficient Wastewater Treatment and Reuse Systems, *Desalination*, **202(1):** 199–206 (2007).

[10] Zentou H., Zainal Abidin Z., Yunus R., Biak D.R.A., Issa M.A., Optimization and Modeling of the Performance of Polydimethylsiloxane for Pervaporation of Ethanol−Water Mixture, *J. Appl. Polym. Sci.*, **138(11):** 1-13 (2020).

[11] Kuvarega A.T., Khumalo N., Dlamini D., Mamba B.B., Polysulfone/N,Pd Co-Doped TiO_2 Composite Membranes for Photocatalytic Dye Degradation, *Sep. Purif. Technol.*, **191:** 122–133 (2018).

[12] Li G., Nandgaonkar A.G., Wang Q., Zhang J., Krause W.E., Wei Q., Lucia L.A., Laccase-Immobilized Bacterial Cellulose/TiO_2 Functionalized Composite Membranes: Evaluation for Photo- and Bio-Catalytic Dye Degradation, *J. Membr. Sci.*, **525:** 89–98 (2017).

Archive of SID.ir

Archive of SID.ir

[13] Yao L., Zhang L., Wang R., Chou S., Dong Z., A New Integrated Approach for Dye Removal From Wastewater by Polyoxometalates Functionalized Membranes, *J. Hazard. Mater.*, **301:** 462–470 (2016).

[14] Foorginezhad S., Zerafat M.M., Microfiltration of Cationic Dyes Using Nano-Clay Membranes, *Ceram. Int.*, **43(17):** 15146–15159 (2017).

[15] Mohtor N.H., Othman M.H.D., Bakar S.A., Kurniawan T.A., Dzinun H., Norddin M.N.A.M., Rajis Z., Synthesis of Nanostructured Titanium Dioxide Layer onto Kaolin Hollow Fibre Membrane via Hydrothermal Method for Decolourisation of Reactive Black 5, *Chemosphere*, **208:** 595–605 (2018).

[16] Hou C., Jiao T., Xing R., Chen Y., Zhou J., Zhang L., Preparation of TiO_2 Nanoparticles Modified Electrospun Nanocomposite Membranes Toward Efficient Dye Degradation for Wastewater Treatment, *J. Taiwan Inst. Chem. Eng.*, **78:** 118–126 (2017).

[17] Mahdavi H.R., Arzani M., Mohammadi T., Synthesis, Characterization and Performance Evaluation of an Optimized Ceramic Membrane with Physical Separation and Photocatalytic Degradation Capabilities, *Ceram. Int.*, **44(9):** 10281–10292 (2018).

[18] Li Y., Zhou J., Fan Y., Ye Y., Tang B., Preparation of Environment-Friendly 3D Eggshell Membrane-Supported Anatase TiO_2 as a Reusable Photocatalyst for Degradation of Organic Dyes, *Chem. Phys. Lett.*, **689:** 142–147 (2017).

[19] Aoudjit L., Martins P.M., Madjene F., Petrovykh D.Y., Lanceros-Mendez S., Photocatalytic Reusable Membranes for the Effective Degradation of Tartrazine with a Solar Photoreactor, *J. Hazard. Mater.*, **344:** 408–416 (2018).

[20] Sahraeian S., Alipour V., Heidari M., Rahmanian O., Karimi Abdolmaleki M., Application of Photocatalytic Process Using UV/TiO_2 for Degradation of Cefepime: a Comparison between Photocatalytic and Photolytic, *Iran. J. Chem. Chem. Eng. (IJCCE)*, **40(3):** 796–803 (2021).

[21] Janarthanan B., Chandrasekaran J., Kumar S., Evaporative Heat Loss and Heat Transfer for Open- and Closed-Cycle Systems of a Floating Tilted Wick Solar Still, *Desalination*, **180(1):** 291–305 (2005).

[22] Zrelli A., Metoui E., Doucouré A., Studying the Effect of Phosphogypsum Addition on Ceramic Membrane Properties, *Eng. Technol. J.*, **41(9):** 1–9 (2023).

[23] Ajari H., Zrelli A., Chaouachi B., Pontié M., Preparation and Characterization of Hydrophobic Flat Sheet Membranes Based on a Recycled Polymer, *Int. Polym. Process.*, **34(3):** 376–382 (2019).

[24] Zrelli A., Elfalleh W., Ghorbal A., Chaouachi B., Valorization of Date Palm Wastes by Lignin Extraction to be Used for the Improvement of Polymeric Membrane Characteristics, *Period. Polytech. Chem. Eng.*, **66(1):** 70–81 (2022).

[25] Feng C., Shi B., Li G., Wu Y., Preparation And Properties of Microporous Membrane from Poly(Vinylidene Fluoride-Co-Tetrafluoroethylene) (F2.4) for Membrane Distillation, *J. Membr. Sci.*, **237(1):** 15–24 (2004).

[26] Li J.-F., Xu Z.-L., Yang H., Yu L.-Y., Liu M., Effect of TiO_2 Nanoparticles on the Surface Morphology and Performance of Microporous PES Membrane, *Appl. Surf. Sci.*, **255(9):** 4725–4732 (2009).

[27] Zrelli A., Bessadok A., Alsalhy Q., Important Parameters of Ceramic Membranes Derived from Oasis Waste and its Application for Car Wash Wastewater Treatment, *J. Membr. Sci. Res.*, **8(1):** 529855 (2022).

[28] Kamgang-Syapnjeu P., Njoya D., Kamseu E., Cornette de Saint Cyr L., Marcano-Zerpa A., Balme S., Bechelany M., Soussan L., Elaboration of a New Ceramic Membrane Support from Cameroonian Clays, Coconut Husks and Eggshells: Application for Escherichia Coli Bacteria Retention, *Appl. Clay Sci.*, **198:** 105836 (2020).

[29] Maleki H., Bertola V., TiO_2 Nanofilms on Polymeric Substrates for the Photocatalytic Degradation of Methylene Blue, *ACS Appl. Nano Mater.*, **2(11):** 7237–7244 (2019).

[30] Babyszko A., Wanag A., Kusiak-Nejman E., Morawski A.W., Effect of Calcination Temperature of SiO_2/TiO_2 Photocatalysts on UV-VIS and VIS Removal Efficiency of Color Contaminants, *Catalysts*, **13(1):** 186 (2023).

[31] Li D.-N., Ma X.-J., Preparation and Photocatalytic Property of Nano-TiO_2 Loaded Activated Carbon Fibers from Iquefued Wood, *WOOD Res.*, **59:** 77-84 (2014).

Archive of SID.ir

Archive of SID.ir

[32] Mishra A., Mehta A., Basu S., Clay Supported TiO_2 Nanoparticles for Photocatalytic Degradation of Environmental Pollutants: a Review, *J. Environ. Chem. Eng.*, **6(5):** 6088–6107 (2018).

[33] Karadimas G., Salonitis K., Ceramic Matrix Composites for Aero Engine Applications—A Review, *Appl. Sci*., **13(5):** 3017 (2023).

[34] Chen Y., Dionysiou D.D., Effect of Calcination Temperature on the Photocatalytic Activity and Adhesion of TiO_2 Films Prepared by the P-25 Powder-Modified Sol–Gel Method, *J. Mol. Catal. Chem.*, **244(1):** 73–82 (2006).

[35] Vrakatseli V., Farsari E., Mataras D., Wetting Properties of Transparent Anatase/Rutile Mixed Phase Glancing Angle Magnetron Sputtered Nano-TiO_2 Films, *Micromachines*, **11(6):** 616 (2020).

[36] Nair A.K., P.E., J., TiO_2 Nanosheet-Graphene Oxide Based Photocatalytic Hierarchical Membrane For Water Purification, *Surf. Coat. Technol.*, **320:** 259–262 (2017).

[37] Aissat M., Hamouda S., Bettahar N., Tarboush B.J.A., Bahmani A., Characterization and Application of Ceramic Membranes Prepared from Algerian Kaolin, *Cerâmica*, **65(376):** 554–561 (2019).

[38] Doke S.M., Yadav G.D., Process Efficacy and Novelty of Titania Membrane Prepared by Polymeric Sol–Gel Method in Removal of Chromium(VI) by Surfactant Enhanced Microfiltration, *Chem. Eng. J.*, **255:** 483–491 (2014).

[39] Phromma S., Wutikhun T., Kasamechonchung P., Eksangsri T., Sapcharoenkun C., Effect of Calcination Temperature on Photocatalytic Activity of Synthesized TiO_2 Nanoparticles via Wet Ball Milling Sol-Gel Method, *Appl. Sci.*, **10(3):** 993 (2020).

[40] Potti P.R., Srivastava V.C., Comparative Studies on Structural, Optical, and Textural Properties of Combustion Derived ZnO Prepared Using Various Fuels and their Photocatalytic Activity, *Ind. Eng. Chem. Res.*, **51(23):** 7948–7956 (2012).

[41] Li Y., Ma G., Peng S., Lu G., Li S., Boron and Nitrogen Co-Doped Titania with Enhanced Visible-Light Photocatalytic Activity for Hydrogen Evolution, *Appl. Surf. Sci*., **254(21):** 6831–6836 (2008).

[42] Luna M., Gatica J.M., Vidal H., Mosquera M.J., Au-TiO_2/SiO_2 Photocatalysts with NO_x Depolluting Activity: Influence of Gold Particle Size and Loading, *Chem. Eng. J.*, **368:** 417–427 (2019).

[43] Li D., Song H., Meng X., Shen T., Sun J., Han W., Wang X., Effects of Particle Size on the Structure and Photocatalytic Performance by Alkali-Treated TiO_2, *Nanomaterials*, **10(3):** 546 (2020).

[44] Ceballos-Chuc M.C., Ramos-Castillo C.M., Rodríguez-Pérez M., Ruiz-Gómez M.Á., Rodríguez-Gattorno G., Villanueva-Cab J., Synergistic Correlation in the Colloidal Properties of TiO_2 Nanoparticles and its Impact on the Photocatalytic Activity, *Inorganics*, **10(9):** 125 (2022).

[45] Retamoso C., Escalona N., González M., Barrientos L., Allende-González P., Stancovich S., Serpell R., Fierro J.L.G., Lopez M., Effect of Particle Size on the Photocatalytic Activity of Modified Rutile Sand (TiO_2) for the Discoloration of Methylene Blue in Water, *J. Photochem. Photobiol. Chem.*, **378:** 136–141 (2019).

[46] Zhu Q., Pan D., Sun Y., Qi D., Controllable Microemulsion Synthesis of Hybrid TiO_2–SiO_2 Hollow Spheres and Au-Doped Hollow Spheres with Enhanced Photocatalytic Activity, *Langmuir*, **38(13):** 4001–4013 (2022).

[47] Ebrahimi F., Nabavi S.R., Omrani A., Fabrication Of PAN/PA6//RgO-TiO_2 Electrospun Nanofibers Membrane with Self-Cleaning Performance under Visible-Light, *J. Appl. Polym. Sci.*, **140(8):** e53523 (2023).

[48] Yerli Soylu N., Soylu A., Dikmetas D.N., Karbancioglu-Guler F., Kucukbayrak S., Erol Taygun M., Photocatalytic and Antimicrobial Properties of Electrospun TiO_2–SiO_2–Al_2O_3–ZrO_2–CaO–CeO_2 Ceramic Membranes, *ACS Omega*, **8(12):** 10836–10850 (2023).

[49] Heredia Deba S.A., Wols B.A., Yntema D.R., Lammertink R.G.H., Advanced Ceramics in Radical Filtration: TiO_2 Layer Thickness Effect on the Photocatalytic Membrane Performance, *J. Membr. Sci.*, **672:** 121423 (2023).

[50] Jaramillo-Fierro X., Gaona S., Ramón J., Valarezo E., Porous Geopolymer/$ZnTiO_3/TiO_2$ Composite for Adsorption and Photocatalytic Degradation of Methylene Blue Dye, *Polymers*, **15(12):** 2697 (2023).

[51] Kusiak-Nejman E., Sienkiewicz A., Wanag A., Rokicka-Konieczna P., Morawski A.W., The Role of Adsorption in the Photocatalytic Decomposition of Dyes on APTES-Modified TiO_2 Nanomaterials, *Catalysts*, **11(2):** 172 (2021).

Archive of SID.ir